ORIGINAL ARTICLE

IJAMB JOURNALAMB.COM
INTERNATIONAL JOURNAL OF ADVANCES IN MEDICAL BIOTECHNOLOGY

Development of PCLMA/HAp-Si composite resin for vat photopolymerization 3D printing

T. N. Palhares[1,2,3*]; J. F. Parreira Lovo[4]; G. Costa Rodrigues[1]; A.Lima Poli[1]; M.A. Sabino[2,5]; R. Rozental[3,6,7]; C.C. Schmitt[1*]

*Corresponding author: E-mail address: thiagonup@gmail.com

Received: October 2024; Accepted: December 2024.

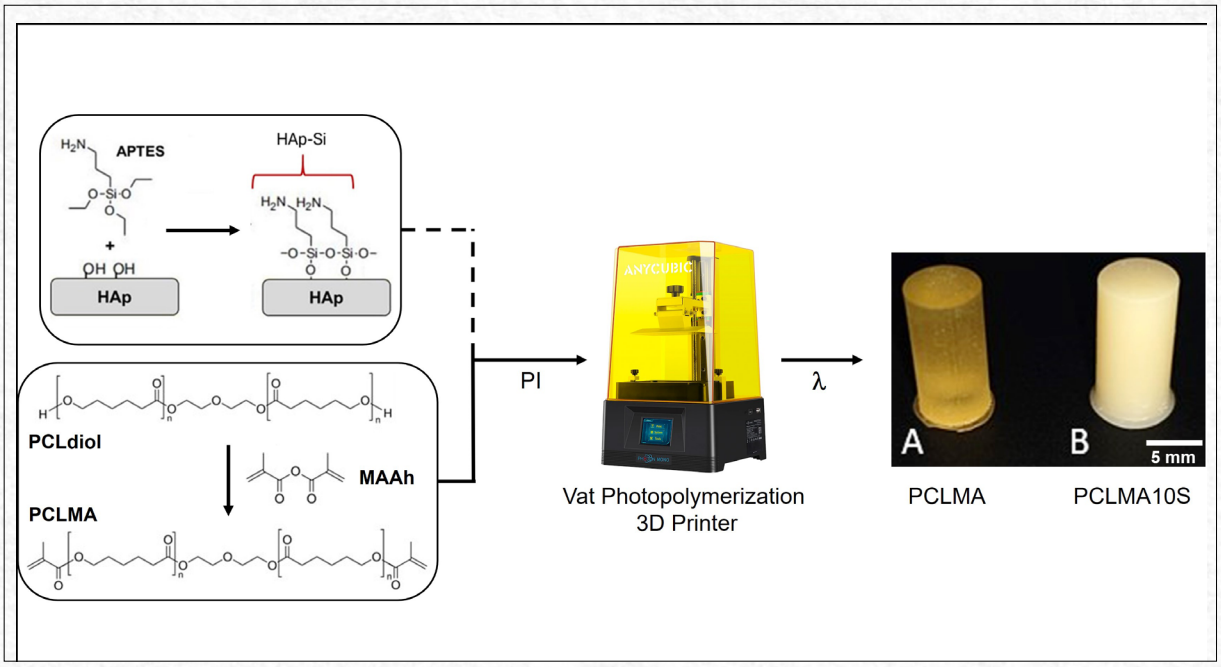

Abstract: The development of bioactive materials for 3D printing has faced significant challenges, particularly in achieving compatibility between organic polymer matrices and inorganic fillers, which is critical for structural stability and biological applications. In this study, a photopolymerizable composite resin based on polycaprolactone methacrylate (PCLMA) was developed, incorporating functionalized hydroxyapatite (HAp-Si) to enhance the phase affinity between the polymer matrix and the inorganic filler. This approach addresses the bottleneck of poor dispersion and weak interfacial interactions commonly reported in the literature for similar systems. Hydroxyapatite was functionalized with 3-aminopropyltrimethoxysilane (APTES), as confirmed by X-ray Diffraction (XRD) and Fourier Transform Infrared Spectroscopy (FTIR), while polycaprolactone diol (PCLdiol) was successfully modified into PCLMA, introducing methacrylate groups and increasing the number-average molecular weight (Mn), also confirmed by FTIR. Scanning Electron Microscopy (SEM) revealed well-dispersed HAp-Si particles, highlighting the improved compatibility and distribution achieved through functionalization. The developed resin exhibited excellent dimensional fidelity during 3D printing of cylindrical samples measuring 6.35 × 12.70 mm. These findings suggest that PCLMA-based composite resins hold promise for advanced vat photopolymerization applications, particularly in tissue engineering and bioactive implant development.

Keywords: Poly(ε-caprolactone) methacrylate. Functionalized hydroxyapatite. Composite resin. Vat photopolymerization. 3D printing

[1]Institute of Chemistry of São Carlos, University of São Paulo (USP), São Carlos, SP, Brazil.
[2]Renato Archer Information Technology Center, Campinas, SP, Brazil.
[3]Technological Development in Health Center, Oswaldo Cruz Institute, Oswaldo Cruz Foundation (FIOCRUZ), Rio de Janeiro, RJ, Brazil.
[4]University Hospital of UFSCar (Ebserh), Federal University of São Carlos, São Carlos, SP, Brazil.
[5]Department of Chemistry, B5IDA Research Group, Simón Bolívar University (USB), Caracas, Venezuela.
[6]Institute of Biomedical Sciences, Federal University of Rio de Janeiro (UFRJ), Rio de Janeiro, RJ, Brazil.
[7]Department of Neuroscience, Albert Einstein College of Medicine, New York, USA.

https://doi.org/10.52466/ijamb.v6i2.133.

Introduction

Among several 3D printing approaches, vat photopolymerization stands out as one of the most precise processes within Additive Manufacturing (AM). This technique enables the production of solid prototypes or end-use objects with high resolution, surface quality, and intricate geometries, using layer heights as fine as 15 to 50 µm. Vat photopolymerization involves curing a photosensitive liquid resin—typically composed of functionalized monomers or oligomers—using a light source in the UV/Vis range (350 to 430 nm), converting the resin into a solid polymer layer by layer [1–3].

The properties and performance of printed objects are directly linked to the composition of the resin. These resins must meet specific physicochemical and mechanical criteria, such as appropriate viscosity for smooth layer deposition, low shrinkage during curing to ensure dimensional stability, and mechanical robustness to withstand the intended application. The fraction of each component, including fillers, significantly influences these properties. Resins used for vat photopolymerization typically consist of monomeric or oligomeric materials—either natural or synthetic—combined with a photoinitiator. They may also include solvents, fillers, light-absorbing dyes, and curing inhibitors to optimize their functionality and achieve the desired performance characteristics[2–7].

The molar mass of a polymer directly influences the printing process, as polymers are frequently functionalized through acrylation or methacrylation of their chains. Typically, a higher degree of crosslinking is achieved with shorter chain lengths, whereas longer chains can lead to reduced crosslinking. On one hand, highly dense crosslinked networks enhance print resolution. On the other hand, an increased molar mass raises the viscosity of the resin, causing difficulties in the 3D printing process. This often necessitates elevated temperatures in the vat or the incorporation of organic solvents, which can introduce challenges such as toxicity, difficulties in complete removal, and contraction of the printed models[8,9].

The polymer/bioceramic composite enhances the properties of both phases and emerges as a promising new material. The effective incorporation of the filler into the polymeric matrix has been the focus of extensive research on composites[10]. Several studies in the literature investigate the mixture of poly(ε-caprolactone) (PCL) and hydroxyapatite (HAp), despite the low phase compatibility between these materials[11,12], particularly when PCL is in the solid state.

PCL is a well-established synthetic polymer with a long history of diverse applications. One of its key advantages is its biocompatibility, characterized by its non-toxic, non-immunogenic nature and low inflammatory response. Another significant benefit is its biodegradability. In vivo, PCL undergoes hydrolytic degradation, producing metabolites such as 6-hydroxyhexanoic acid, CO_2, and H_2O, which are easily eliminated via the respiratory and urinary systems. Its degradation rate ranges from 2 to 4 years, making it a highly promising material for 3D-printed scaffolds. Additionally, PCL is notable for its favorable mechanical properties, ease of processing, and compatibility with other polymeric and ceramic materials[13–15].

Hydroxyapatite (HAp) is classified as a calcium phosphate bioceramic, with a structure and functionality comparable to those found in bone and dental tissues. Due to its inherent biocompatibility and bioactivity, HAp is widely used as an implant material and has the property to induce osteogenic differentiation[16–19].

The stoichiometry of hydroxyapatite (HAp) is commonly represented as $Ca_5(PO_4)_3OH$ or, considering its crystallographic unit cell, $Ca_{10}(PO_4)_6(OH)_2$ corresponding to a theoretical Ca/P ratio of 1.67 for stoichiometric HAp. However, in practical terms, HAp can exhibit a variable gram atom Ca/P ratio, ranging from 1.5 (tricalcium phosphate, $Ca_3(PO_4)_2$) to 2.0 (tetracalcium phosphate, $Ca_4(PO_4)_2CaO$) as observed in calcium phosphate phase diagrams. This variability reflects the compositional and structural changes that can occur during synthesis or processing[20–22].

This underscores the importance of improving the affinity of the ceramic filler to the polymeric matrix through surface modification processes, such as silanization. This process involves coating a hydroxylated surface with a silane to alter its properties. For example, 3-aminopropyltrimethoxysilane (APTES) can be used to modify HAp by hydrolyzing the ethoxy groups and forming a siloxane layer on its surface[23,24]. Additionally, the aminopropyl group present on the surface of HAp promotes interactions with polymeric matrices when combined[11].

The functionalization of hydroxyapatite (HAp) is a well-established strategy to enhance its integration into composite materials, particularly in improving its compatibility with polymer matrices. Among various functionalization methods, the use of 3-aminopropyltrimethoxysilane (APTES) offers notable advantages. One key benefit of silanizing HAp with APTES is the enhancement of its biocompatibility. While HAp is inherently biocompatible, the introduction of amine ($-NH_2$) groups reduces its surface energy, increasing compatibility with cellular wall proteins. This improvement facilitates better cell adhesion, proliferation, and differentiation—critical factors for tissue regeneration. Additionally, the formation of polysiloxanes on the HAp surface contributes to increased hardness, strength, and stability, further reinforcing its mecha-

nical properties. The aminopropyl groups present on the silanized HAp surface also promote interaction with polymer matrices, ensuring improved dispersion and physical integrity of the composite scaffolds. These advantages highlight the versatility of APTES functionalization in creating advanced materials for biomedical applications[23–25].

The literature indicates that even at low filler content, photocurable resin systems mixed with HAp can exhibit poor dispersion and agglomeration[26], which is undesirable for vat photopolymerization processes. Conversely, adding filler percentages above 20% can also pose challenges, as it may affect the performance of the 3D printing machine, particularly if it is an LCD-type printer[27], This is especially true unless dispersing agents or rheological processing aids are employed, which can subsequently interfere with optimal polymerization.

In this context, the present study developed a composite resin for 3D printing via photopolymerization. The research focused on formulating a composite resin using poly(ε-caprolactone) methacrylate (PCLMA) as the matrix, incorporating either silanized hydroxyapatite (HAp-Si) functionalized with APTES or hydroxyapatite (HAp) as fillers. Poly(ε-caprolactone) (PCL) is widely recognized for its biocompatibility, biodegradability, and suitability for biomedical applications, particularly in tissue engineering, due to its ability to support cell adhesion and proliferation. Similarly, hydroxyapatite (HAp) is a well-established biomaterial, known for its osteoconductive and bioactive properties, which mimic the mineral component of bone tissue, making it ideal for bone regeneration applications. By combining these intrinsic properties with tailored functionalization, this study aims to develop a potentially biocompatible material that exhibits enhanced phase affinity, mechanical stability, and suitability for complex 3D-printed structures in biomedical applications.

Methodology

Synthesis of hydroxyapatite

Hydroxyapatite (HAp) was synthesized using a wet precipitation method, maintaining a theoretical ion ratio of $[Ca]^{2+}/[PO_4]^{3-}$ = 1.67. A solution of diammonium hydrogen phosphate ($(NH_4)_2HPO_4$) (purity ≥99.0%, Sigma-Aldrich, Saint Louis, United States) was slowly added to a calcium nitrate solution ($Ca(NO_3)_2{\cdot}4H_2O$) (purity ≥99.0%, Sigma-Aldrich, Saint Louis, United States) under constant stirring and heating at 90°C. After the complete addition of the phosphate solution, the pH of the reaction was kept between 10 and 11 by the controlled addition of concentrated ammonium hydroxide (NH_4OH) (purity ≥99.0%, Sigma-Aldrich, Saint Louis, United States)[28–30].

The mixture was then vacuum filtered using a Büchner funnel. The resulting solid was washed with ultrapure water until the filtrate reached a neutral pH. The solid was subsequently lyophilized, ground into a powder, and sieved through a 90 µm mesh before being stored in a desiccator.

Functionalization of HAp via silanization with 3-Aminopropyltriethoxysilane (APTES)

The silanization reaction was performed to modify the surface of the hydroxyapatite (HAp). Approximately 1 g of HAp was added to an aqueous solution containing 40 ml of ethanol (P.A.) (purity >96%, Êxodo Cientifica, Sumaré, Brazil) and 10 ml of distilled water, then sonicated for 2 hours at 60 °C to initiate the hydrolysis of alkoxy groups and to deagglomerate the particles. Subsequently, 2.21 g of 3-aminopropyltriethoxysilane (APTES) (purity ≥99.0%, Sigma-Aldrich, Saint Louis, United States) was dissolved in 50 ml of ethanol (P.A.) and stirred for 30 minutes. This solution was then added to the HAp mixture and stirred for an additional 3 hours. The pH was adjusted to 9-10 with ammonium hydroxide (NH_4OH) (purity ≥99.0%, Sigma-Aldrich, Saint Louis, United States), and the reaction was allowed to continue for another 3 hours. After filtering the mixture through filter paper, the powder was initially dried at room temperature and then cured at 130 °C to strengthen the silane coating by forming a polysiloxane network structure[24,31–33]. Figure S1 illustrates this reaction.

Finally, the product was washed repeatedly until the filtrate reached a neutral pH. The solid was then lyophilized, ground into a powder, and sieved through a 90-100 µm mesh before being stored in a desiccator. The silanized hydroxyapatite is hereafter referred to as HAp-Si.

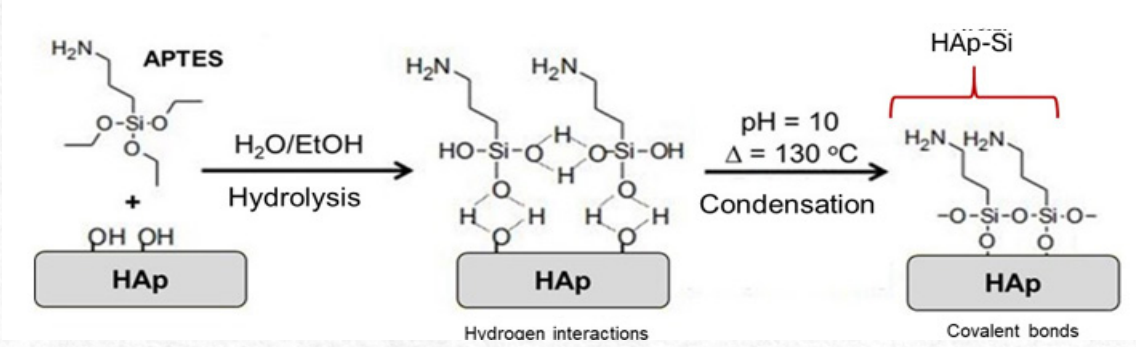

Figure S1 - Silanization functionalization reaction of APTES on HAp Surface
Source: adapted from Kataoka, Shiba, Tagaya, 2019(17))

Methacrylation of poly(ε-caprolactone) diol

The methacrylation of poly(ε-caprolactone) diol oligomer (PCLdiol) (purity >97%, Sigma-Aldrich, Saint Louis, United States) was achieved through a reaction with methacrylic anhydride (MAAh) (purity ≥94.0%, Sigma-Aldrich, Saint Louis, United States), following methods described in the literature(8,34). Figure S2 illustrates the methacrylation reaction scheme.

The following protocol was employed: The oligomer was dissolved in dichloromethane (DCM) (purity ≥99.8%, Êxodo Científica, Sumaré, Brazil) at 100% of its weight. A 30% molar excess of MAAh and a 30% molar amount of triethylamine (TEA) (purity ≥99.0%, Êxodo Científica, Sumaré, Brazil) per hydroxyl terminal group were added, with TEA serving to neutralize the methacrylic acid formed during the reaction. The methacrylation was carried out at room temperature under a nitrogen atmosphere for 24 hours. After the reaction was complete, DCM, excess MAAh, TEA, and the methacrylic acid formed were removed by precipitating the methacrylated oligomer in cold isopropanol (purity ≥99.0%, Êxodo Científica, Sumaré, Brazil). The methacrylated oligomer was then centrifuged, washed with distilled water, separated, and lyophilized. The resulting methacrylated product was identified as poly(ε-caprolactone) dimethacrylate resin (PCLMA).

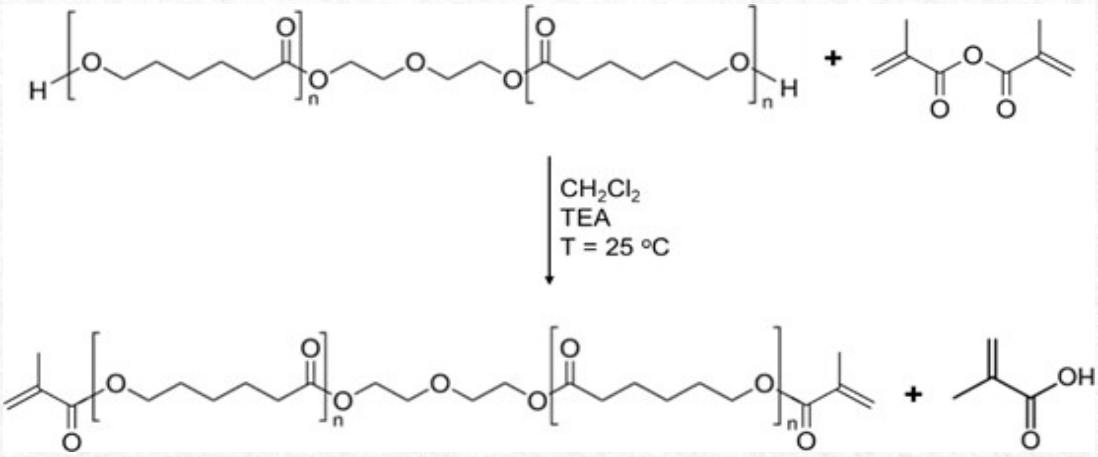

Figure S2 - Methacrylation reaction of PCLdiol to modify and obtain PCLMA.

X-ray Diffraction (XRD) of HAp and HAp-Si

XRD analysis was performed on both HAp and HAp-Si to identify their crystalline structures and assess any modifications resulting from the silanization process. The powder samples were re-sieved to prevent agglomeration. XRD patterns were obtained using a BRUKER APEX II Duo diffractometer with CuKα radiation (λ = 1.5418 Å) at room temperature, over a 2θ range of 10° to 70°.

Fourier Transform Infrared Spectroscopy (FTIR)

Transmission-mode FTIR was performed to identify structural changes resulting from the chemical modifications of both HAp and PCLdiol. Fourier Transform Infrared (FTIR) spectroscopy was conducted over a wavenumber range of 4000 to 400 cm^{-1} at room temperature, using KBr in a 1:100 ratio. Data acquisition was carried out on a Shimadzu IR Affinity 1 spectrophotometer, utilizing 32 scans and a resolution of 4 cm^{-1}.

Determination of average molar mass by Gel Permeation Chromatography (GPC) of PCLdiol and PCLMA

The molar mass of PCLdiol and PCLMA was determined using gel permeation chromatography to compare the increase in molar mass resulting from the modification of the polymer matrix. This technique provided values for the number-average molar mass (Mn), weight-average molar mass (Mw), and polydispersity (Đ), where Đ = Mw/Mn.

The analyses were conducted using a Shimadzu chromatograph equipped with LC-20AD pumps, a CBM-20A controller, a CTO-20A oven, and an RID-10A detector. The analytical conditions included a flow rate of 1 mL/min, a temperature of 35 °C, a duration of 50 minutes, and tetrahydrofuran (THF) (Sigma-Aldrich, Saint Louis, United States) as the mobile phase, with sample injection concentrations of 10 mg/mL. The stationary phase consisted of four Waters Styragel columns in series (HR 4E and HR 5E) with rigid particles of poly(styrene-co-divinylbenzene) copolymer. A standard calibration curve was created to quantify the molar mass as a function of elution time, using poly(methyl methacrylate) and polystyrene standards, with injection concentrations of 5 mg/mL.

Preparation of photocurable composites of PCLMA and HAp-Si

PCLMA was utilized as the polymer matrix to prepare composite samples mixed with either HAp or HAp-Si as fillers. The materials were weighed in the different mass proportions and sonicated for 30 minutes. Subsequently, the photoinitiator Irgacure 369 (purity >97%, Sigma-Aldrich, Saint Louis, United States) was added at 3 wt% of PCLMA and stirred for 12 hours using a magnetic stirrer to ensure the dispersion and homogeneity of the samples. These mixtures were stored in amber vials, kept in the dark, and away from any light sources to prevent unwanted premature polymerization. This process resulted in a viscous liquid photocurable resin, which serves as the input for 3D printing via photopolymerization.

Based on these considerations, this research prepared photocurable composites with only 10% inorganic filler (either HAp or HAp-Si) as a first approximation. These composites were identified as follows: dimethacrylated PCL (PCLMA), PCLMA + 10% HAp (w/w) (PCLMA10), and PCLMA + 10% HAp-Si (w/w) (PCLMA10S).

Rheology of PCLMA resins and composites PCLMA10 and PCLMA10S

The viscosity of the resins is a crucial parameter for ensuring good printability. Viscosity measurements (Pa·s) were conducted as a function of shear rate (1/s) on samples of PCLMA and its composites, PCLMA10 and PCLMA10S. Additionally, a commercial resin (Anycubic/Standard Clear Resin), which is from the same brand as the 3D LCD printer used in this study, was included for comparison. The experiments were performed using a TA Instruments DHR-2 rheometer with a parallel plate of 25 mm diameter and 0.5 mm spacing at 25 °C.

Scanning Electron Microscopy with Energy Dispersive X-ray Spectroscopy (SEM-EDX) of PCLMA and Composites PCLMA10 and PCLMA10S

Scanning Electron Microscopy (SEM) analyses with Energy Dispersive X-ray Spectroscopy (EDX) were conducted using a JEOL JSM-7200F microscope to verify the dispersion, morphology, and size of the filler particles within the polymer matrix. EDX was specifically employed to identify the composition of the inorganic filler and confirm the presence of HAp. The cured materials were frozen in liquid nitrogen and then fractured. They were subsequently affixed to the surface of metallic stubs using carbon tape, which possesses both adhesive and conductive properties. The stubs containing the samples were coated with carbon to enhance conductivity for image acquisition. Images of the samples were obtained using a secondary electron detector, with a potential difference of 15 kV applied for electron acceleration.

Thermogravimetric Analysis / Derivative Thermogravimetric Analysis (TG/DTG) of PCLMA and composites PCLMA10 and PCLMA10S

This analysis was performed to confirm the

addition of filler and to identify the mass value present in each composite formulation. TG/DTG measurements were obtained using a TA Instruments TGA Q50 thermogravimetric analyzer, with approximately 10 to 15 mg of sample in the heating range from 25 to 1000 °C, at a heating rate of 10 °C/min under a nitrogen atmosphere at a flow rate of 50 mL/min

3D printing process by photopolymerization of cylindrical samples

Cylindrical samples with a height (H) of 12.70 mm and a diameter (D) of 6.35 mm were prepared in triplicates. The commercial 3D printer Anycubic Photon Mono was utilized for the subsequent tests in this study. The 3D printing process was conducted through photopolymerization using the Liquid Crystal Display (LCD) technique, employing an LED projector with a nominal wavelength of 405 nm, a resolution of 2560 x 1620 pixels (2K; XY: 0.051 mm; Z: 0.01 mm), a nominal power of 45 W, and a print envelope of 130 x 80 x 165 mm.

The basic printing parameters included a layer height of 0.03 mm (30 micrometers) and a curing time per layer of 6 seconds. Upon completion, the printed models were washed with isopropanol, dried, and subjected to a UV bath using the Anycubic Wash&Cure 2.0 equipment for 1 minute to finalize the curing of residual oligomers. An analysis of variance (ANOVA) with Tukey's test ($\alpha = 0.05$) was performed using OriginLab software to evaluate and compare the grouping of the obtained means.

Results and Discussion

X-ray Diffraction (XRD) Analysis of HAp and HAp-Si

The XRD diffractogram presented in Figure 1 exhibits well-defined peaks, identifying the primary crystalline phases of hydroxyapatite (HAp) at 2θ = 25.89° (002); 28.18° (102); 28.96° (210); 31.84° (211); 32.90° (112); 34.07° (300); 35.46° (202); 39.27° (212); and 39.80° (310). These findings corroborate those reported in the literature(35,36).

Additionally, the results for HAp-Si indicate that silanization did not alter the crystalline structure of the material(30,37). This observation can be attributed to the degree of grafting, which occurred primarily on the surface of the inorganic particles, as illustrated in Figure S1.

Infrared Spectroscopy by Fourier Transform (FTIR) HAp, HAp-Si, and APTES

The FTIR spectra of HAp, HAp-Si, and APTES are depicted in Figure 2. The functional group bands characteristic of HAp and APTES are evident in HAp-Si, aligning with those reported in the literature. The bands identified in HAp correspond to $-PO_4^{3-}$ (565, 605, 875, 962, and 1033 cm^{-1}) and -OH (3570 cm^{-1}). For APTES, the prominent bands include C-N (1589 cm^{-1}), $-CH_2-$ (2930 cm^{-1}), and $-NH_2$ (3372 cm^{-1})[23,38,39].

Although the Si-O-C (1107 cm^{-1}) and Si-O-Si (1080 cm^{-1}) bands are strong and predominant in APTES, they were overshadowed by the $-PO_4^{3-}$ bands of HAp due to the lower concentration of the silane in the material. Analysis of the HAp-Si spectrum revealed the presence of the primary bands from both materials, as previously mentioned. This observation suggests that the silanization reaction of the HAp surface facilitated by APTES has indeed occurred, a finding that will be further corroborated by the forthcoming.

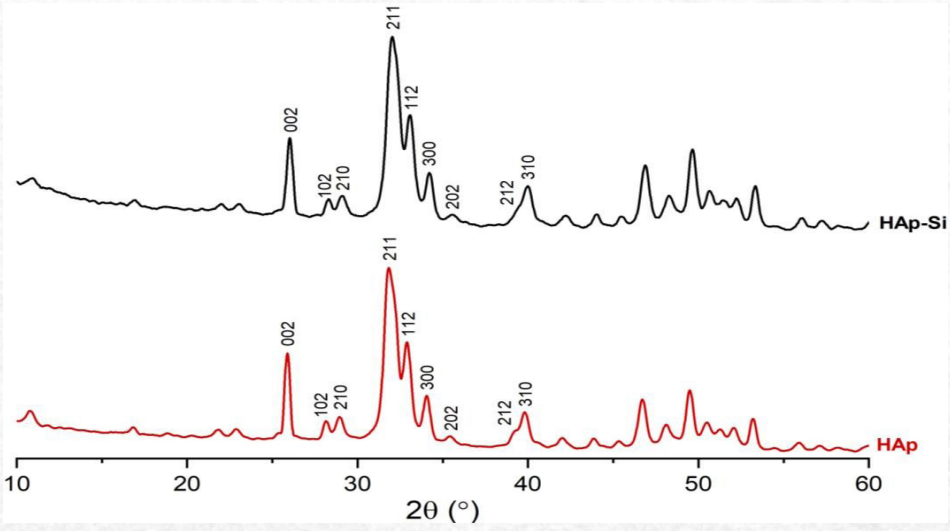

Figure 1 - X-ray Diffraction (XRD) analysis of HAp and HAp-Si.

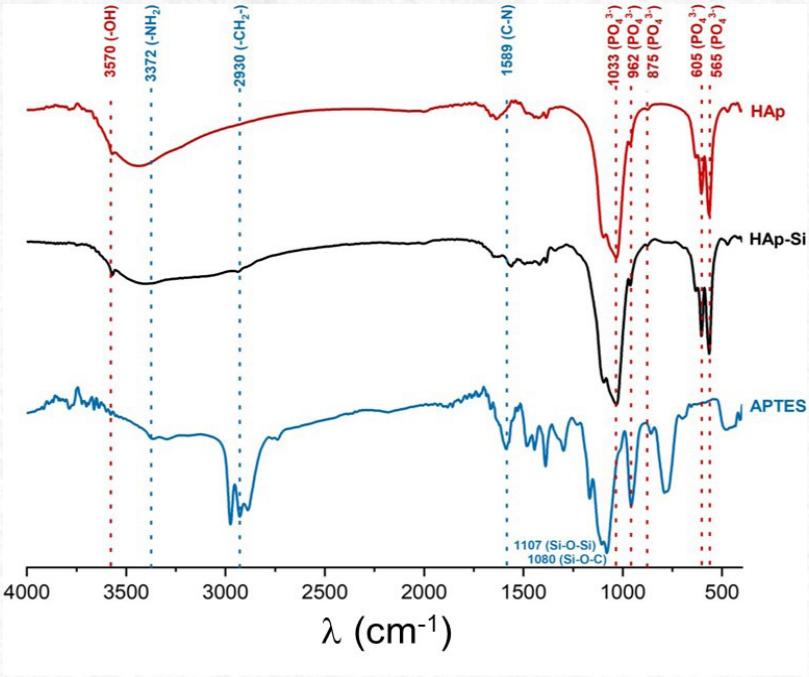

Figure 2 - FTIR Spectra of HAp, HAp-Si, and APTES

MAAh, PCLMA, and PCLdiol

In Figure 3, the absorption band at 1635 cm^{-1} in the PCLMA spectrum corresponds to the vinyl group (H_2C=CH-) introduced during the methacrylation of PCLdiol with methacrylic anhydride (MAAh). Additionally, the hydroxyl (-OH) absorption band, observed around 3500 cm^{-1} in the PCLdiol spectrum, shows a significant reduction in the PCLMA spectrum due to the substitution of hydroxyl groups during the methacrylation process[37,40].

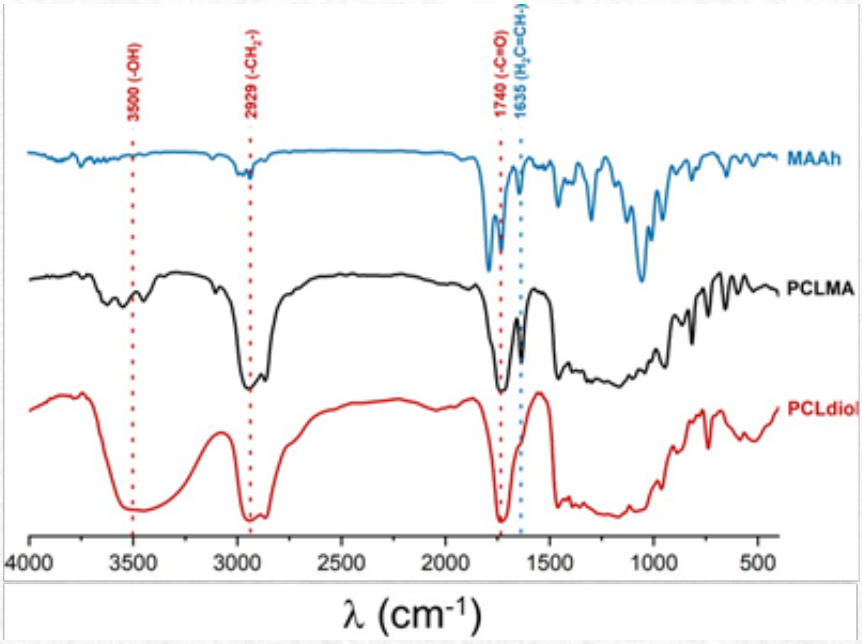

Figure 3 - Fourier Transform Infrared (FTIR) Spectroscopy of PCLdiol, PCLMA, and MAAh Resin.

Molar mass by gel permeation chromatography (GPC) of PCLdiol and PCLMA Resin

The molar mass values were determined to elucidate the variation in the distribution of the PCLdiol resin and its functionalized counterpart, PCLMA. The results for the number-average molar mass (Mn), weight-average molar mass (Mw), and polydispersity (Đ), as determined by Gel Permeation Chromatography (GPC), are presented in Table 1. The Mn of PCLdiol was measured at 668 g/mol, aligning reasonably well with the nominal value of 530 g/mol reported by the manufacturer.

It is important to emphasize that organic synthesis, particularly polymerization reactions, inherently produces a distribution of molecular weights described by a normal distribution curve, rather than a single exact value. The reported Mn represents the average of this distribution, explaining the slight deviation from the manufacturer's specification. For PCLMA, the Mn increased to 826 g/mol, confirming the successful substitution of hydrogen atoms in the terminal hydroxyl groups with methacrylate groups.

The polydispersity index (Đ) for PCLMA was determined to be 1.47, which is comparable to the Đ value of 1.71 for PCLdiol. A dispersity index close to 1 reflects favorable properties such as improved uniformity of polymer chains, enhanced processability, and better overall material performance. These characteristics are particularly advantageous for polymers designed for advanced applications, including additive manufacturing technologies[41].

Thermogravimetric Analysis (TGA) and Differential Thermogravimetry (DTG) of PCLMA resins and composites PCLMA10 and PCLMA10S

Thermal analysis by TGA was employed to characterize the thermal decomposition profile of the PCLMA resin and its composites, PCLMA10 and PCLMA10S, as illustrated by the curves in Figure 4. This analysis also aimed to estimate the inorganic residue content to evaluate the filler proportion in each resin aliquot and to compare it with the intended theoretical composition.

The residual content values provide estimates of the inorganic filler, specifically the HAp phase, in the PCLMA10 and PCLMA10S composites. In all samples, the curves exhibited a single stage of thermal degradation commencing at temperatures above

Table 1 - Values of Number-Average Molar Mass (Mn), Weight-Average Molar Mass (Mw), and polydispersity (Đ).

Sample	Mn (g/mol)	Mw (g/mol)	Đ
PCLdiol	668.0	1148.0	1.71
PCLMA	826.0	1214.0	1.47

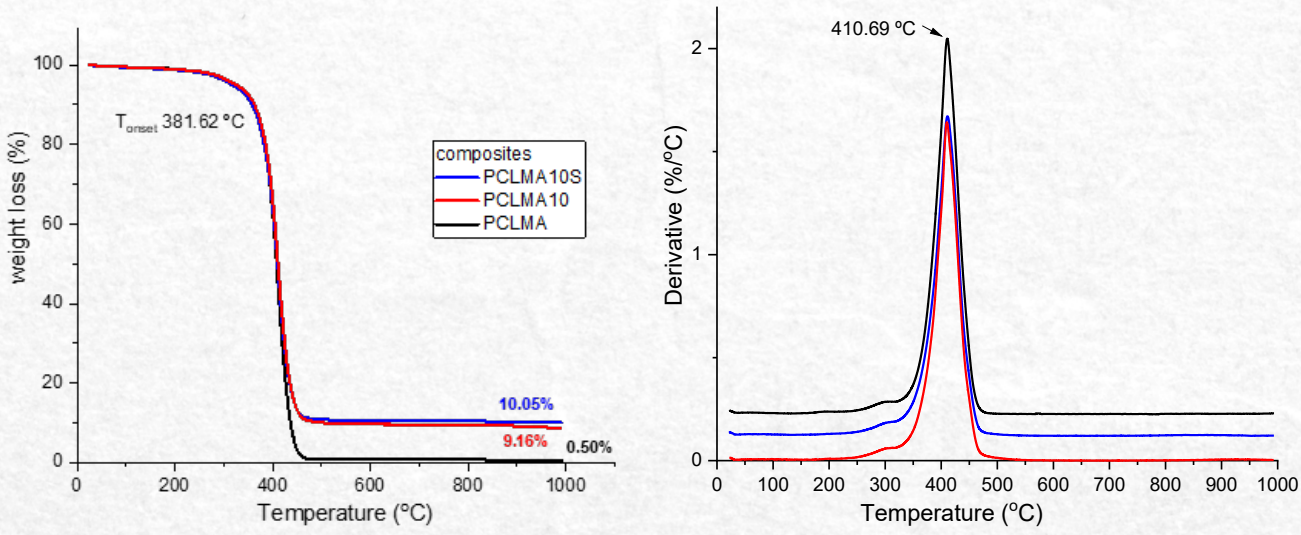

Figure 4 - TGA and DTG Curves of PCLMA Resin and Composites PCLMA10 and PCLMA10S

250 °C, which corresponds to the decomposition of the polymer matrix. A second degradation phase was noted just above 400 °C, confirming the presence of a binary composite with only the filler incorporated in the PCLMA polymer matrix. The onset temperature, indicating the estimated temperature at which material degradation begins, was approximately 381.6 °C for all samples.

The theoretical filler values in the samples reflect the fraction of each sample, indicating variability in filler dispersion and homogeneity throughout the polymer phase. The values in parentheses presented at the end of the curves represent the residual filler content related to the mass loss of HAp (~9.16%) and HAp-Si (~10.1%). The DTG curve indicates that the maximum degradation rate occurs at approximately 410 °C for all samples. Notably, the addition of HAp or HAp-Si did not influence the thermal degradation rate of the polymer matrix.

Rheology of PCLMA resins and composites (PCLMA10 and PCLMA10S)

Viscosity is a critical parameter for 3D resin printing through photopolymerization. During printing, the resins need to continuously fill the voids formed by the platform displacement in each layer. Several factors influence high-resolution 3D printing by photopolymerization. Generally, the resin viscosity must be low enough, depending on the molar mass of the monomer/oligomer, to allow detachment of the cured layers from the printing vat. It's also important for the resin to maintain certain pseudoplasticity required for forming a dimensionally stable 3D piece with adequate elastic-plastic behavior[42]. Otherwise, adhesive forces from the process will cause delamination between the cured layers of the printed object. Additionally, low viscosity resins may allow for higher printing speeds, which could be necessary for small dimensions or high productivity pieces[9,43].

The viscosity as a function of shear rate for PCLMA resins and the composites PCLMA10 and PCLMA10S was measured at 25°C and is presented in Figure 5. The rheological curves for PCLdiol, PCLMA, PCLMA10, and PCLMA10S resins, along with the commercial Anycubic resin at room temperature (~25°C), demonstrate a viscous fluid behavior. Specifically, the viscosity of PCLdiol, PCLMA, PCLMA10, and PCLMA10S samples reaches a plateau at shear rates between 500 and 1000 s^{-1}, indicating that they behave as Newtonian fluids with constant viscosity as the shear rate varies. At lower shear rates, ranging from 0 to 500 s^{-1}, the samples exhibit pseudoplastic behavior, which is essential for printing processes to ensure good shape fidelity[44].

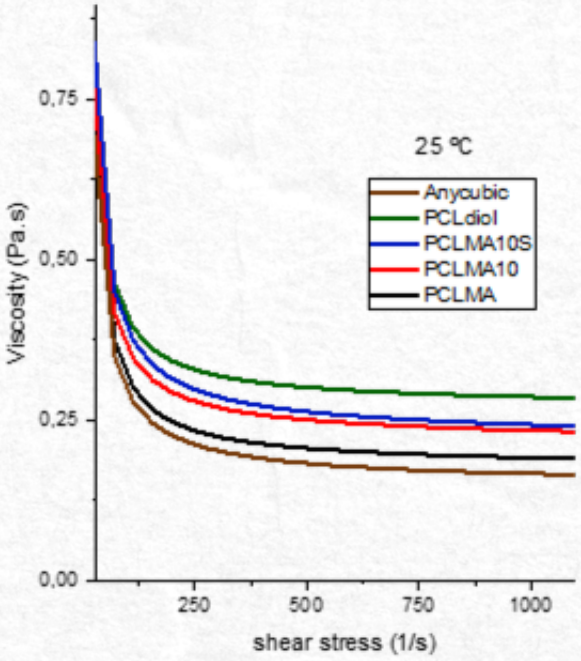

Figure 5 - Viscosity as a function of shear rate for PCLMA resins and PCLMA10 and PCLMA10S composites.

Scanning Electron Microscopy with Energy Dispersive Spectroscopy (SEM-EDX) of the composites

Scanning Electron Microscopy (SEM-EDX) was employed to investigate the morphology of HAp

and HAp-Si fillers dispersed within the PCLMA matrix. This analysis aimed to measure the area of the agglomerates and individual particles, as well as to map and chemically identify the presence of fillers by detecting carbon (C), oxygen (O), calcium (Ca), and phosphorus (P).

Figure 6 presents a cross-sectional view obtained through cryogenic fracture of the cylindrical samples. For the matrix of modified PCLMA, certain marks are observed on the surface of the cryogenic cut, which could also be related to some brittleness induced by the modification made, given that it is known that PCL is a polymer with ductile behavior. At higher magnifications, the presence of inorganic fillers in the composite samples PCLMA10 e PCLMA10S is evident, for magnifications of 200X and 1500X, the presence of the hydroxyapatite phase is evident as dispersed inorganic particles are observed in the polymeric matrix. It is also evident that the fracture propagation pattern for the PCLMA10 composite is different, as a distinct pattern of cryogenic fracture propagation is observed, possibly inducing a certain brittleness to the material.

From Figure 6, it is evident that filler agglomerates formed and coalesced, exhibiting different shapes and sizes, which resulted PCLMA10 in a heterogeneous material. However, in the PCLMA10S sample containing modified hydroxyapatite (HAp-Si), the dispersion process proved to be more effective, demonstrating good distribution of the particles within the PCLMA polymer matrix. This suggests a reduction in interfacial tension between the organic and inorganic phases[45], indicating enhanced compatibility that could improve the printability of 3D structures and possibily improve their mechanical performance[46].

Crosby and Lee (2007) assert that mixing polymers with fillers introduces significant complexities regarding their form. Achieving homogeneous composites with good dispersion and distribution remains a formidable challenge. The addition of excess filler reduces the average distance between particles, thereby increasing the likelihood of collisions and the formation of micrometer-scale aggregates. This phenomenon can result in a loss of the characteristic properties of the material and an increase in its dimensions[47,48].

Figure 7 presents the EDX analysis conducted at a magnification of 6,500x, focusing on specific points to confirm that the particles observed in the SEM images are indeed hydroxyapatite (HAp). This is evidenced by the detection of calcium (Ca) and phosphorus (P) in their composition. In the case of PCLMA10S, the detection of silicon (Si) further corroborates the successful functionalization of the HAp with APTES.

The HAp used was not subjected to thermal treatment via sintering, which typically promotes crystalline organization and adjusts the composition toward the stoichiometric Ca/P ratio of 1.67. Instead, the synthesized HAp retained a less crystalline and more amorphous structure, leading to a Ca/P ratio of 1.79, as determined by EDX analysis. This deviation from stoichiometry can arise from residual amorphous calcium phosphate phases or an excess of calcium ions incorporated during synthesis.

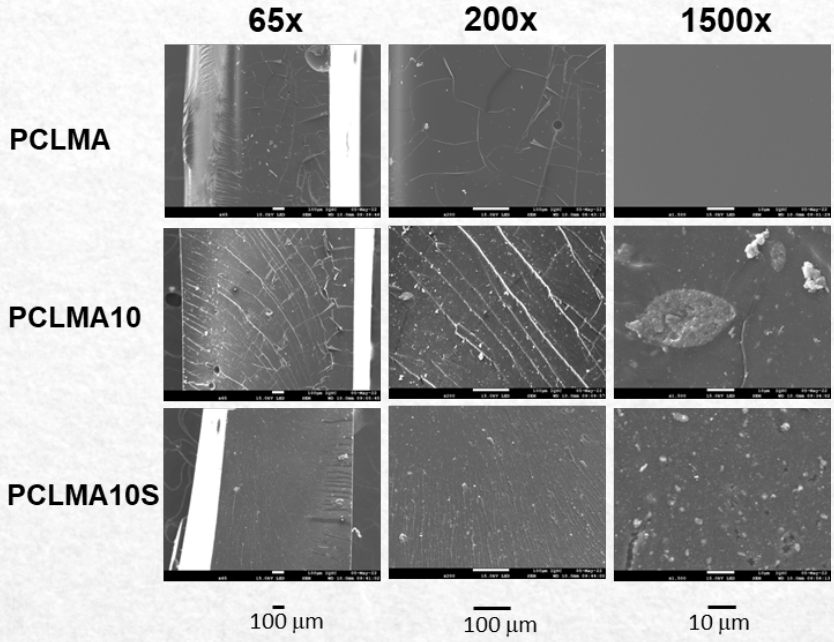

Figure 6 - SEM of fractured cross-section of composites with and without fillers

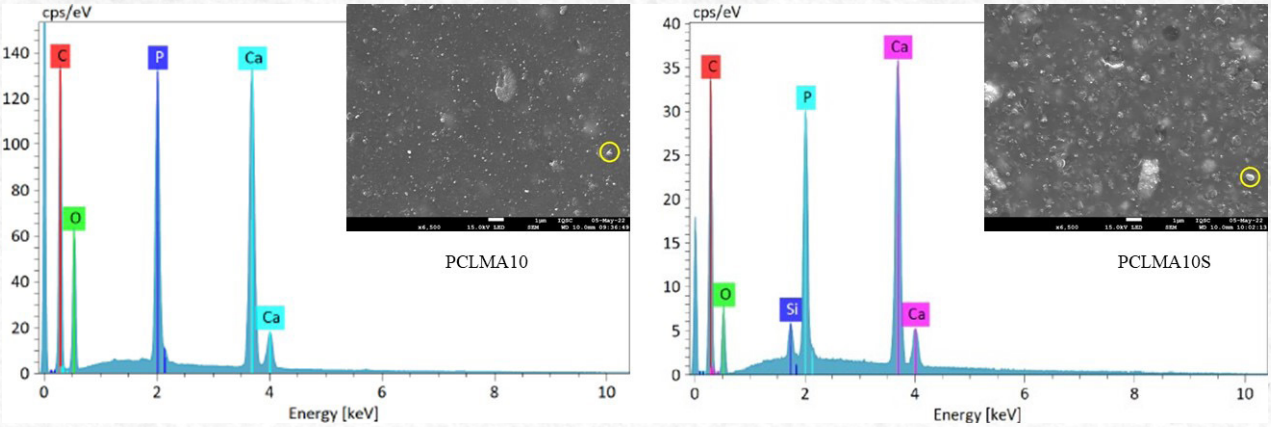

Figure 7 - EDX analysis at 6500x magnification of fractured samples of PCLMA, PCLMA10, and PCLMA10S.

3D Printing process by photopolymerization

Printing tests were conducted to validate the feasibility of printing solid cylindrical structures. As shown in Figure 8, for comparative purposes, the printing was carried out for the PCLMA resin (A) and the composite PCLMA10S (B), as the composite with HAp-Si exhibited favorable rheological behavior and good morphology between the phases. It can be observed that for a simple cylindrical geometry, the process of 3D structure formation demonstrates efficiency.

The color differences observed in the samples are notable. The PCLMA resin exhibited a translucent yellow/golden hue, while the PCLMA10S composite presented an opaque, milky appearance, visually confirming the dispersion of the filler (HAp-Si) throughout the polymer matrix. This contrast underscores the impact of the inorganic filler on the optical characteristics of the composite.

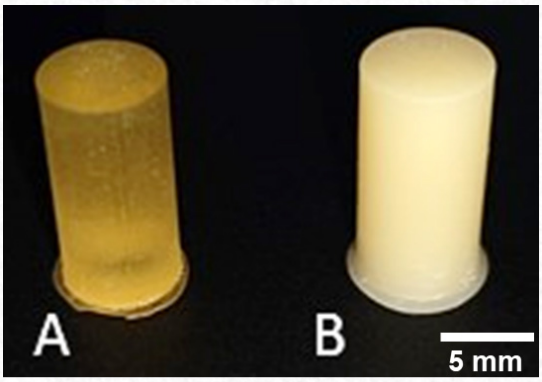

Figure 8 - 3D printing of cylindrical samples of a) PCLMA and b) PCLMA10S.

Accuracy evaluation of 3D printing cylindrical samples

3D printing resins and materials must possess the necessary precision to match the dimensions of the planned 3D model. The designed samples, with a height (H) of 12.70 mm and a diameter (D) of 6.35 mm, were printed and subsequently compared. The average error (e) was calculated using Equations 2 and 3[49].

$$e_D = D - d \quad \text{(Eq. 2)}$$

$$e_H = H - h \quad \text{(Eq. 3)}$$

Where, = average diameter error (mm);

e_D = average diameter error (mm);

D = 3D model diameter (mm);

d = 3D printed sample diameter;

e_H = average height error (mm);

H = 3D model height (mm);

h= 3D printed sample height (mm)..

Table 2 presents the measured diameters and heights of the compression test samples, along

with their respective associated errors.

The results indicate effective light penetration through the subsequent layers of all test samples. Furthermore, the average height for each sample was adequate for them to be categorized in the same group ("a") according to ANOVA analysis.

Regarding the diameter measurements, the test samples made from the PCLMA resin exhibited the most significant deviation from the designed dimensions, thus belonging to group "A" in the ANOVA analysis. In contrast, the average diameters of the PCLMA10S and PCLMA10 samples were closer to the intended 6.35 mm, placing them in group "B." Based on the previously observed results, dimensional fidelity in printing was confirmed.

Table 2 - Average diameter and height of compression test samples and associated error.

Sample	Average Diameter (mm)	e_D (mm)	Average Height (mm)	e_H (mm)
PCLMA	6.180 ± 0.045 A*	-0.170 (-2.68 %)	12.678 ± 0.005 a*	-0.022 (-0.04 %)
PCLMA10S	6.384 ± 0.022 B	+0.034 (+0.54 %)	12.672 ± 0.005 a	-0.028 (-0.04 %)
PCLMA10	6.396 ± 0.009 B	+0.046 (+0.72 %)	12.678 ± 0.014 a	-0.022 (-0.11 %)

Conclusions

This study demonstrated the successful synthesis of hydroxyapatite (HAp) and its functionalization with APTES to form HAp-Si, as confirmed by X-ray Diffraction (XRD) and Fourier Transform Infrared Spectroscopy (FTIR). The efficient conversion of PCLdiol into polycaprolactone methacrylate (PCLMA) was also verified through FTIR, with the introduction of methacrylate groups enabling photopolymerization via Irgacure 369.

Scanning Electron Microscopy (SEM) revealed dispersed HAp agglomerates, and Energy-Dispersive X-ray Spectroscopy (EDX) indicated a Ca/P ratio of 1.79, slightly deviating from the stoichiometric value due to the absence of post-sinterization treatment. Functionalization improved filler dispersion and its interaction with the polymer matrix.

Cylindrical 3D-printed PCLMA composite samples were fabricated successfully, demonstrating the potential of PCLMA-based photopolymerizable resins for advanced applications. Future studies should further investigate mechanical properties, biocompatibility, and the suitability of complex structures for clinical use, particularly in tissue engineering and bioactive implant development.

Acknowledgements

To the esteemed Dr. Jorge Vicente Lopes da Silva, who is regarded as an exemplary professional and a person of indisputable character. We are profoundly grateful for the opportunities and the freedom you granted us to explore 3D printing. Your legacy continues to inspire, and you will always be remembered with deep admiration and respect.

Fundação Oswaldo Cruz (Fiocruz) - Processo Fiocruz n° 25380.002400/2021-96 and INOVA PRODUCTS (grant #6320360368) and to the esteemed Rodrigo Correa (VPPIS-Fiocruz) in association with the Brazilian Ministry of Health; São Paulo Research Foundation (FAPESP – grant #2023/14057-6, grant # 2022/15211-6, and grant #2021/13949-5); and Program CNPq (grant # 301211/2024-8 and grant # 311184/2022-7).

References

[1]. Quan H, Zhang T, Xu H, Luo S, Nie J, Zhu X. Photo-curing 3D printing technique and its challenges. Bioact Mater. 2020 Mar;5(1):110–5.

[2]. Ressler A, Zakeri S, Konnunaho P, Schwentenwein M, Levänen E, Frankberg EJ. Cleaning strategies for 3D-printed porous scaffolds used for bone regeneration fabricated via ceramic vat photopolymerization. Ceram Int. 2024 Oct;

[3]. Enayati-Gerdroodbar A, Khayati A, Ahmadi M, Pourabbas B, Ali Aboudzadeh M, Salami-Kalajahi M. An overview on potential of novel photoinitiators for vat photopolymerization-based 3D/4D printing formulations. Eur Polym J. 2024 Dec;221:113552.

[4]. Bao Y, Paunović N, Leroux J. Challenges and Opportunities in 3D Printing of Biodegradable Medical Devices by Emerging Photopolymerization Techniques. Adv Funct Mater. 2022 Apr 19;32(15).

[5]. Paunović N, Bao Y, Coulter FB, Masania K, Geks AK, Klein K, et al. Digital light 3D printing of customized bioresorbable airway stents with elastomeric properties. Sci Adv. 2021 Feb 5;7(6).

[6]. She Y, Fan Z, Wang L, Li Y, Sun W, Tang H, et al. 3D Printed Biomimetic PCL Scaffold as Framework Interspersed With Collagen for Long Segment Tracheal Replacement. Front Cell Dev Biol. 2021 Jan 21;9.

[7]. Ding Y, Ikura R, Yamaoka K, Nishida K, Sugawara A, Uyama H, et al. Reinforcement and Controlling the Stability of Poly(ε-caprolactone)-Based Polymeric Materials via Reversible and Movable Cross-Links Employing Cyclic Polyphenylene Sulfide. ACS Macro Lett. 2024 Oct 15;13(10):1265–71.

[8]. Green BJ, Worthington KS, Thompson JR, Bunn SJ, Rethwisch M, Kaalberg EE, et al. Effect of Molecular Weight and Functionality on Acrylated Poly(caprolactone) for Stereolithography and Biomedical Applications. Biomacromolecules. 2018 Sep 10;19(9):3682–92.

[9]. van Bochove B, Hannink G, Buma P, Grijpma DW. Preparation of Designed Poly(trimethylene carbonate) Meniscus Implants by Stereolithography: Challenges in Stereolithography. Macromol Biosci. 2016 Dec 17;16(12):1853–63.

[10]. Palhares TN, Menezes LR de, Kronemberger GS, Borchio PG de M, Baptista LS, Pereira L da CB, et al. Production and Characterization of Poly (Lactic Acid)/Nanostructured Carboapatite for 3D Printing of Bioactive Scaffolds for Bone Tissue Engineering. 3D Print Addit Manuf. 2021 Aug 1;8(4):227–37.

[11]. Biggemann J, Müller P, Köllner D, Simon S, Hoffmann P, Heik P, et al. Hierarchical Surface Texturing of Hydroxyapatite Ceramics: Influence on the Adhesive Bonding Strength of Polymeric Polycaprolactone. J Funct Biomater. 2020 Oct 3;11(4):73.

[12].Aminatun, Sujak M. K. A, Izak R. D, Hadi S, Sari YW, Gunawarman, et al. Fabrication and biocompatibility evaluation of hydroxyapatite–polycaprolactone–gelatin composite nanofibers as a bone scaffold. RSC Adv. 2024;14(34):24815–27.

[13].Thijssen Q, Cornelis K, Alkaissy R, Locs J, Damme L Van, Schaubroeck D, et al. Tough Photo-Cross--Linked PCL-Hydroxyapatite Composites for Bone Tissue Engineering. Biomacromolecules. 2022 Mar 14;23(3):1366–75.

[14].Shah SR, Modi CD, Singh S, Mori DD, Soniwala MM, Prajapati BG. Recent Advances in Additive Manufacturing of Polycaprolactone-Based Scaffolds for Tissue Engineering Applications: A Comprehensive Review. Regen Eng Transl Med. 2024 Sep 18;

[15]. La Fuente CIA, Maniglia BC, Tadini CC. Biodegradable polymers: A review about biodegradation and its implications and applications. Packaging Technology and Science. 2023 Feb 26;36(2):81–95.

[16]. Balasooriya IL, Chen J, Korale Gedara SM, Han Y, Wickramaratne MN. Applications of Nano Hydroxyapatite as Adsorbents: A Review. Nanomaterials. 2022 Jul 6;12(14):2324.

[17]. Baptista LS, Kronemberger GS, Côrtes I, Charelli LE, Matsui RAM, Palhares TN, et al. Adult Stem Cells Spheroids to Optimize Cell Colonization in Scaffolds for Cartilage and Bone Tissue Engineering. Int J Mol Sci. 2018 Apr 25;19(5):1285.

[18].Kronemberger GS, Palhares TN, Rossi AM, Verçosa BRF, Sartoretto SC, Resende R, et al. A Synergic Strategy: Adipose-Derived Stem Cell Spheroids Seeded on 3D-Printed PLA/CHA Scaffolds Implanted in a Bone Critical-Size Defect Model. J Funct Biomater. 2023 Nov 21;14(12):555.

[19].Dornelas J, Dornelas G, Rossi A, Piattelli A, Di Pietro N, Romasco T, et al. The Incorporation of Zinc into Hydroxyapatite and Its Influence on the Cellular Response to Biomaterials: A Systematic Review. J Funct Biomater. 2024 Jun 28;15(7):178.

[20].Wopenka B, Pasteris JD. A mineralogical perspective on the apatite in bone. Materials Science and Engineering: C. 2005 Apr;25(2):131–43.

[21].Omelon SJ, Grynpas MD. Relationships between Polyphosphate Chemistry, Biochemistry and Apatite Biomineralization. Chem Rev. 2008 Nov 12;108(11):4694–715.

[22].Narasaraju TSB, Phebe DE. Some physico-chemical aspects of hydroxylapatite. J Mater Sci. 1996;31(1):1–21.

[23].Marycz K, Kornicka-Garbowska K, Patej A, Sobierajska P, Kotela A, Turlej E, et al. Aminopropyltriethoxysilane (APTES)-Modified Nanohydroxyapatite (nHAp) Incorporated with Iron Oxide (IO) Nanoparticles Promotes Early Osteogenesis, Reduces Inflammation and Inhibits Osteoclast Activity. Materials. 2022 Mar 11;15(6):2095.

[24].Kataoka T, Shiba K, Tagaya M. Design of Hydroxyapatite-Based Multifunctional Nanoparticles for Cell Labelling and Cell Growth Inhibition. Regen Med Front. 2019;2(1).

[25].Sypabekova M, Hagemann A, Rho D, Kim S. Review: 3-Aminopropyltriethoxysilane (APTES) Deposition Methods on Oxide Surfaces in Solution and Vapor Phases for Biosensing Applications. Biosensors (Basel). 2022 Dec 27;13(1):36.

[26].Kennedy BM, De Barra E, Hampshire S, Kelleher MC. Investigation of oleic acid as a dispersant for hydroxyapatite powders for use in ceramic filled photo-curable resins for stereolithography. J Eur Ceram Soc. 2023 Dec;43(15):7146–66.

[27].Yao Y, Sha N, Zhao Z. Highly Concentrated Hydroxyapatite Suspension for DLP Printing. IOP Conf Ser Mater Sci Eng. 2019 Nov 1;678(1):012016.

[28].de Oliveira Lomelino R, Castro-Silva II, Linhares ABR, Alves GG, de Albuquerque Santos SR, Gameiro VS, et al. The association of human primary bone cells with biphasic calcium phosphate (βTCP/HA 70:30) granules increases bone repair. J Mater Sci Mater Med. 2012 Mar 27;23(3):781–8.

[29].Gasperini FM, Calasans-Maia MD, Resende RFB,

Granjeiro JM, Rossi AM, Lopes RT, et al. Bone-nanohydroxyapatite spheres interface evaluation by synchrotron radiation X-ray microfluorescence. X-Ray Spectrometry. 2012 Jan 21;41(1):6–11.

[30].Michelot A, Sarda S, Audin C, Deydier E, Manoury E, Poli R, et al. Spectroscopic characterisation of hydroxyapatite and nanocrystalline apatite with grafted aminopropyltriethoxysilane: nature of silane–surface interaction. J Mater Sci. 2015 Sep 5;50(17):5746–57.

[31].Atak BH, Buyuk B, Huysal M, Isik S, Senel M, Metzger W, et al. Preparation and characterization of amine functional nano-hydroxyapatite/chitosan bionanocomposite for bone tissue engineering applications. Carbohydr Polym. 2017 May;164:200–13.

[32].Goonasekera CS, Jack KS, Cooper-White JJ, Grøndahl L. Attachment of poly(acrylic acid) to 3-aminopropyltriethoxysilane surface-modified hydroxyapatite. J Mater Chem B. 2013;1(42):5842.

[33].Russo L, Taraballi F, Lupo C, Poveda A, Jiménez--Barbero J, Sandri M, et al. Carbonate hydroxyapatite functionalization: a comparative study towards (bio)molecules fixation. Interface Focus. 2014 Feb 6;4(1):20130040.

[34].Elomaa L, Teixeira S, Hakala R, Korhonen H, Grijpma DW, Seppälä J V. Preparation of poly(ε-caprolactone)--based tissue engineering scaffolds by stereolithography. Acta Biomater. 2011 Nov;7(11):3850–6.

[35].Nejati E, Mirzadeh H, Zandi M. Synthesis and characterization of nano-hydroxyapatite rods/poly(l--lactide acid) composite scaffolds for bone tissue engineering. Compos Part A Appl Sci Manuf. 2008 Oct;39(10):1589–96.

[36].Tian G, Zhu G, Xu S, Ren T. A novel shape memory poly(ε-caprolactone)/hydroxyapatite nanoparticle networks for potential biomedical applications. J Solid State Chem. 2019 Apr;272:78–86.

[37].Cai L, Wang S. Poly(ε-caprolactone) acrylates synthesized using a facile method for fabricating networks to achieve controllable physicochemical properties and tunable cell responses. Polymer (Guildf). 2010 Jan;51(1):164–77.

[38].Lucia A, Bacher M, van Herwijnen HWG, Rosenau T. A Direct Silanization Protocol for Dialdehyde Cellulose. Molecules. 2020 May 25;25(10):2458.

[39].Salim SA, Loutfy SA, El-Fakharany EM, Taha TH, Hussien Y, Kamoun EA. Influence of chitosan and hydroxyapatite incorporation on properties of electrospun PVA/HA nanofibrous mats for bone tissue regeneration: Nanofibers optimization and in-vitro assessment. J Drug Deliv Sci Technol. 2021 Apr;62:102417.

[40].Risangud N, Jiraborvornpongsa N, Pasee S, Kaewkong P, Kunkit N, Sungkhaphan P, et al. Poly(ester- co -glycidyl methacrylate) for digital light processing in biomedical applications. J Appl Polym Sci. 2021 Sep 10;138(42).

[41].Zhu Y, Ramadani E, Egap E. Thiol ligand capped quantum dot as an efficient and oxygen tolerance photoinitiator for aqueous phase radical polymerization and 3D printing under visible light. Polym Chem. 2021;12(35):5106–16.

[42].Peñas MI, Calafel MI, Aguirresarobe RH, Tierno M, Conde JI, Pascual B, et al. How Is Rheology Involved in 3D Printing of Phase-Separated PVC-Acrylate Copolymers Obtained by Free Radical Polymerization. Polymers (Basel). 2020 Sep 12;12(9):2070.

[43].Murphy CA, Lim KS, Woodfield TBF. Next Evolution in Organ-Scale Biofabrication: Bioresin Design for Rapid High-Resolution Vat Polymerization. Advanced Materials. 2022 May 24;34(20).

[44].Kuang X, Zhao Z, Chen K, Fang D, Kang G, Qi HJ. High-Speed 3D Printing of High-Performance Thermosetting Polymers via Two-Stage Curing. Macromol Rapid Commun. 2018 Apr 31;39(7).

[45].Goonasekera CS, Jack KS, Cooper-White JJ, Grøndahl L. Dispersion of hydroxyapatite nanoparticles in solution and in polycaprolactone composite scaffolds. J Mater Chem B. 2016;4(3):409–21.

[46].Šupová M. Problem of hydroxyapatite dispersion in polymer matrices: a review. J Mater Sci Mater Med. 2009 Jun 20;20(6):1201–13.

[47].Crosby AJ, Lee J. Polymer Nanocomposites: The "Nano" Effect on Mechanical Properties. Polymer Reviews. 2007 Apr;47(2):217–29.

[48].Lee JY, Zhang Q, Emrick T, Crosby AJ. Nanoparticle Alignment and Repulsion during Failure of Glassy Polymer Nanocomposites. Macromolecules. 2006 Oct 1;39(21):7392–6.

[49].Lee JS, Park HS, Jung H, Lee H, Hong H, Lee YJ, et al. 3D-printable photocurable bioink for cartilage regeneration of tonsil-derived mesenchymal stem cells. Addit Manuf. 2020 May;33:101136.